

# Shock-enhanced ammonia emission in the Egg nebula

Dinh-V-Trung<sup>1</sup>, P.J. Chiu<sup>2</sup>, Jeremy Lim

*Institute of Astronomy and Astrophysics, Academia Sinica  
P.O Box, 23-141, Taipei 106, Taiwan*

trung@asiaa.sinica.edu.tw, pjchiu@asiaa.sinica.edu.tw,  
jlim@asiaa.sinica.edu.tw

## ABSTRACT

We present high angular resolution observations of the  $\text{NH}_3(1,1)$ ,  $(2,2)$  and  $(3,3)$  inversion transitions from the Egg Nebula, the archetypical proto-planetary nebula. The spatial distribution and kinematics of the emission in all three lines show four distinct components or lobes that are aligned with the polar and equatorial directions. The kinematics of the  $\text{NH}_3$  emission is also found to follow a clear pattern: redshifted emission in the South and West and blueshifted emission in the North and East. The morphology and spatial kinematics of  $\text{NH}_3$  emission are shown to have strong similarity to that observed previously in molecular hydrogen emission and CO emission which arise from the shocked molecular gas. We also find that the higher lying inversion transition  $\text{NH}_3(2,2)$  and  $(3,3)$  are stronger in the polar direction in comparison to the lower transition  $\text{NH}_3(1,1)$ . We conclude that the  $\text{NH}_3$  emission traces the warm molecular gas, which is shocked and heated by the interaction between the high velocity outflows and the surrounding envelope. The presence of strong ammonia emission associated with the shock fronts and the lack of the emission at the center of the nebula indicate that the abundance of ammonia is significantly enhanced by shocks, a situation very similar to that found in outflows from protostars.

*Subject headings:* ISM: planetary nebula: general — ISM: planetary nebula: individual: CRL2688 — ISM: molecules

---

<sup>1</sup>on leave from Center for Quantum Electronics, Institute of Physics, Vietnamese Academy of Science and Technology, 10 DaoTan, ThuLe, BaDinh, Hanoi, Vietnam

<sup>2</sup>Institute of Astronomy, National Central University No. 300, Jhongda Rd, Jhongli City, Taoyuan County 320, Taiwan

## 1. Introduction

The Egg nebula (CRL 2688) is widely considered as the prototype of proto-planetary nebulae (PPN), a class of stars in the rapid transition phase between the AGB and planetary nebulae. During the PPN phase the central post-AGB star contracts and gradually becomes hotter, but is not yet hot enough to ionize its surrounding envelope. Using high resolution spectroscopic observations of the scattered stellar light Klochkova et al. (2000) determine a spectral type F5Ia for the central star with an effective temperature of  $T_{\text{eff}}=6500\text{K}$ . The abundance analysis reveals the enrichment of C and N together with strong enhancement of slow neutron capture (s-process) elements, as expected for the carbon rich post-AGB star at the center of the Egg nebula. Jura & Kroto (1990) suggest that the central star left the AGB a few hundreds years ago. The last episode of high mass loss rate at the end of the AGB phase, commonly referred as the superwind phase, has created a massive circumstellar envelope around the central post-AGB star. As a result, the Egg nebula is a strong source of continuum and molecular emissions. Numerous and strong molecular lines have been detected by Young et al. (1992), Truong-Bach et al. (1988). From continuum emission Jura et al. (2001) inferred a gas mass of  $\sim 0.2 M_{\odot}$  scaled to the distance of 420 pc recently determined by Ueta et al. (2006).

High spatial resolution optical images of CRL 2688 reveal a pair of bipolar lobes seen as search-light beams emanating from the central (obscured) star and oriented perpendicular to a prominent dark lane (Sahai et al. 1998a). This conspicuous dark lane has been commonly interpreted as an equatorial disk of cold dust. High angular resolution images of hot molecular hydrogen gas emission at  $2.2 \mu\text{m}$  reveal shocked gas, tracing the strong interaction between the fast outflows and the slow wind (Sahai et al. 1998b). Surprisingly, hot molecular hydrogen emission is seen in both bipolar lobes as well as in the equatorial plane far beyond the dark lane, indicating the presence of multiple fast collimated outflows. The presence of high velocity outflows has also been inferred from the detection of high velocity wings in the strong emission lines of CO and CS molecules by Young et al. (1992).

Indeed, high spatial resolution mapping of CO J=2–1 emission by Cox et al. (2000) reveals the presence of several pairs of collimated fast molecular outflows along both the bipolar axis and the equatorial plane. Surprisingly, these molecular outflows can be traced back to a common origin, presumably the location of the central post-AGB star in the Egg nebula. Cox et al. (2000) suggest that the observed CO emission does not constitute the actual fast collimated outflows, but rather molecular gas swept up by even faster collimated outflows that comprise mainly atomic or ionized gas. In contrast to its appearance in the optical, no equatorial disk is the Egg nebula is seen in the CO J=2–1 by Cox et al. (2000). High spatial resolution observation of the high density tracer HCN J=1–0 by Bieging &

Nguyen-Q-Rieu (1996) indicates higher gas density along both the bipolar lobes and the equatorial plane, consistent with the hypothesis that the molecular gas is swept up by the interaction with the fast outflows.

Ammonia ( $\text{NH}_3$ ) is known to exist in many different environments. The inversion transitions of  $\text{NH}_3$  which are closely spaced in frequency can be detected and imaged at high angular resolution almost simultaneously, allowing quite straightforward excitation analysis (Ho & Townes 1983). The detected inversion lines from metastable levels  $J=K$  can be used as a natural thermometer to constrain the temperature of the molecular gas (Walmsley & Ungerechts 1983). The (1,1) and (2,2) inversion transitions in the Egg nebula were first detected in single dish observations of Nguyen-Q-Rieu et al. (1984). Follow-up observations by Truong-Bach et al. (1988) also detected the higher excitation lines (3,3) and (4,4). Subsequent high angular resolution observation of the  $\text{NH}_3(1,1)$  line by Nguyen-Q-Rieu (1986) indicates that  $\text{NH}_3$  is distributed in a disk-like structure lying along the dark lane with a faint spur extending from the center of the disk to the north. Nguyen-Q-Rieu et al. (1986) suggest that the  $\text{NH}_3$  emission is confined in a disk or more probably in a torus oriented perpendicular to the optical lobes. The torus, which has a diameter of  $\sim 12''$  and a thickness less than  $3''$ , is expanding at a velocity of  $\sim 15 \text{ km s}^{-1}$ . The low sensitivity and low velocity resolution of the observation by Nguyen-Q-Rieu et al. (1986), however, preclude any firm conclusion on the spatial kinematics of the ammonia in the Egg nebula.

In this paper we report high angular resolution observations of  $\text{NH}_3$  inversion lines (1,1), (2,2) and (3,3) to determine the spatial kinematics and to probe the physical conditions inside the molecular envelope of the Egg nebula.

## 2. Observations and Data Reduction

We carried out the observations of the Egg nebula in the  $\text{NH}_3(1,1)$ ,  $\text{NH}_3(2,2)$  and  $\text{NH}_3(3,3)$  inversion lines using the Very Large Array (VLA<sup>3</sup>). The  $\text{NH}_3(3,3)$  line was observed on March 6, 2003 and  $\text{NH}_3(1,1)$  and  $\text{NH}_3(2,2)$  were observed simultaneously on July 18, 2004. All the observations were done in the most compact configuration of VLA. The phase center of our observations was  $\alpha_{j2000}=21\text{h}02\text{m}18.6\text{s}$ ,  $\delta_{j2000}=36\text{d}41\text{m}37.8\text{s}$ , which is the same as the peak of the continuum emission observed previously by Cox et al. (2000). To observe these lines we configured the VLA correlator in the 1A mode with 12.5 MHz bandwidth in 64 channels, thus providing a channel width of 195.3 kHz or a velocity resolution of

---

<sup>3</sup>The National Radio Astronomy Observatory is a facility of the National Science Foundation operated under a cooperative agreement by Associated Universities, Inc.

2.45  $\text{kms}^{-1}$  over a useful velocity coverage of  $\sim 150 \text{ kms}^{-1}$ . We monitored the nearby quasar 21095+35330 at frequent intervals (every 5 minutes or so) to correct for the antennas gain variations caused primarily by atmospheric fluctuations. The stronger quasars 2253+161 was used to correct for the shape of the bandpass and its variation with time. The absolute flux scale of our observations was determined from observation of standard quasar 0137+331 (3C48). The data were edited, calibrated and mapped using AIPS data reduction package. The calibrated visibilities are then Fourier transformed to form the DIRTY images. The natural weighting is used throughout. The DIRTY images were deconvolved using normal clean algorithm implemented in AIPS. In order to get better signal-to-noise ratio we smooth the data to a velocity resolution of 4.9  $\text{kms}^{-1}$  per channel. The rms noise level are  $\sim 2.0$ , 1.5 and 1.5  $\text{mJy beam}^{-1}$  for the  $\text{NH}_3(1,1)$ , (2,2) and (3,3) line, respectively. The difference of rms level in three lines is because of the integration time and weather conditions are different. Table 1 provides a summary of our VLA observations.

### 3. Results

Using the VLA we successful imaged the  $\text{NH}_3(1,1)$ , (2,2), and (3,3) inversion transitions in the Egg nebula. In Figure 1, 2 and 3 we show the channel maps of the  $\text{NH}_3$  emission. The emission in each of the three transitions cover a velocity range between  $-74$  to  $-4 \text{ kms}^{-1}$ . The morphology of the emission is broadly consistent with the lines forming in an expanding environment because the emission is most compact at the extreme blueshifted and redshifted velocity channels and becomes progressively more extended in velocity channels around the systemic velocity of  $V_{\text{LSR}} = -35 \text{ kms}^{-1}$  inferred by Truong-Bach et al. (1988) from the observations of a number of molecular lines in the Egg nebula . We integrate all the emission above  $2\sigma$  level in the channel maps of the (1,1), (2,2) and (3,3) lines. The resulting total intensity profiles are presented in Figure 4. Clearly the strength and the shape of all

Table 1: Summary of the VLA observations

	$\text{NH}_3(1,1)$	$\text{NH}_3(2,2)$	$\text{NH}_3(3,3)$
Obs. date	July 18, 2004	July 18, 2004	March 06, 2003
Int. time	1 hour	1 hour	1 hour
Clean beam	$3''.5 \times 3''.1$	$4''.1 \times 3''.4$	$3''.6 \times 3''$
	PA = $44^\circ.3$	PA = $74^\circ.7$	PA = $44^\circ.5$
$\Delta V$ ( $\text{kms}^{-1}$ )	4.9	4.9	4.9
noise level	2.0	1.5	1.5
( $\text{mJy beam}^{-1}$ )			

three  $\text{NH}_3$  lines are almost identical. The line shape is not the usual parabola, which is typical for an optically thick line formed in an expanding spherical circumstellar envelope. Instead, the line profiles have a triangular shape, reflecting the more peculiar kinematics and spatial distribution of ammonia in the Egg nebula. These three lines of ammonia were observed previously using the single dish telescope by Nguyen-Q-Rieu et al. (1984) and Truong-Bach et al. (1988). Using a conversion factor of  $\sim 0.73 \text{ Jy K}^{-1}$  appropriate for the Effelsberg 100m radio telescope at the frequencies of the  $\text{NH}_3$  lines, we estimate that the peak flux in the (1,1) and (3,3) lines is  $\sim 60 \text{ mJy}$ , similar to that seen in our VLA observations (see Figure 4). The strength of the (2,2) line as observed by Nguyen-Q-Rieu et al. (1984) is slightly weaker than the other two lines. In our VLA observations we find that the strength of the (2,2) line is almost the same as that for the (1,1) and (3,3) lines. It is likely that the relative weakness of the (2,2) in the single dish observation might be due to either calibration and/or the low S/N of the single dish data. Therefore, we conclude that our VLA observations have recovered all the flux in all three inversion lines of ammonia.

It's well known that each of the inversion lines of ammonia has complex hyperfine structure. However, the hyperfine splitting is only significant for the (1,1) line (Kukolich 1967). The hyperfine structure of the (1,1) line consists of the main line group and four groups of satellite lines, which are shifted in velocity in either direction by  $\sim 8$  and  $\sim 20 \text{ kms}^{-1}$ . Assuming the the hyperfine lines are optically thin and form under LTE condition, the intensity of the satellite groups at  $\pm 20 \text{ kms}^{-1}$  is about 20% of that for the main line (Kukolich 1967, Rydbeck et al. 1977). Because the peak flux of the (1,1) line is about  $\sim 10\sigma$  in the velocity channels  $-43.6 \text{ kms}^{-1}$  and  $-48.6 \text{ kms}^{-1}$ , where the rms noise level  $\sigma = 2 \text{ mJy beam}^{-1}$ , the contribution to the intensity of the line in other velocity channels such as  $-23.9 \text{ kms}^{-1}$  and  $-28.8 \text{ kms}^{-1}$  due to the hyperfine splitting is approximately is  $\sim 2\sigma$ . This contribution due to hyperfine structure is modest in comparison to the observed (1,1) lines intensity in the abovementioned velocity channels. As a result, we conclude that hyperfine structure in the (1,1) line does not affect significantly the discussion on the spatial distribution of the emission and also the velocity structure of the  $\text{NH}_3$  in the Egg nebula.

Close inspection of the channel maps reveals that the spatial distribution and kinematics of the emission in three transitions of  $\text{NH}_3$  are very similar. We can clearly separate the ammonia emission into four components having distinct spatial-kinematics, which will be referred as the north, south, east and west lobes. The north and south lobes are most easily seen in the blueshifted and redshifted velocity channels between  $-53$  to  $-68 \text{ kms}^{-1}$  and  $-4$  to  $-24 \text{ kms}^{-1}$ , respectively. These components extend to the north and south of the center of the nebula along the bipolar axis as defined in the optical images. In the channel maps of all three lines, only the north lobe can be seen as distinct. The south lobe is a protrusion connected to the stronger east lobe. The east and west lobes can be seen prominently in

the velocity channels between  $-29$  to  $-48 \text{ kms}^{-1}$  straddling the systemic velocity. These components are stronger in intensity and aligned in the equatorial direction of the nebula. In all three lines the intensity of the emission from the east lobe is dominant over other components. We note that the east and west lobes are located on either side of the center of the nebula where there is a general lack of emission. That can be seen notably in the central velocity channel at  $-34 \text{ kms}^{-1}$  of  $\text{NH}_3$  (1,1) and (3,3) lines shown in Figures 1 and 3.

We integrate all the emission stronger than  $2\sigma$  in the channel maps to produce the integrated intensity maps of all three  $\text{NH}_3$  lines. The maps are shown in Figures 5, 6 and 7. The  $\text{NH}_3$  emission in all three lines shows a cross-like shape, especially in  $\text{NH}_3(3,3)$ . The cross-like shape is the natural result of the presence of four components identified in the channel maps. The total spatial extent of the emission is about  $\sim 14''$  in both the polar direction and the equatorial direction. We note that the north and south lobes appear distinct and more prominent in ortho- $\text{NH}_3(3,3)$  transition than in lower lying para- $\text{NH}_3$  transitions (1,1) and (2,2). Comparing to previous observation of Nguyen-Q-Rieu et al. (1986), we can see that the dramatic improvement in sensitivity of the VLA allows us to detect the fainter emission in the north and south lobes and provides the full picture of the  $\text{NH}_3$  distribution in the Egg nebula.

To investigate the kinematics of the  $\text{NH}_3$  emission we form the intensity-weighted mean velocity maps of all three lines using all the emission stronger than  $4\sigma$  level in the channel maps. The resulting maps are also shown in Figures 5, 6 and 7. In all three lines the north and south lobes exhibit opposite mean velocity, i.e. the emission in the north lobe is entirely blue-shifted and that in the south lobe is entirely red-shifted. These two lobes in the polar direction are almost mirror symmetric in spatial morphology and mean velocity with respect to the center of the nebula. In the equatorial direction, the kinematics of the east and west lobes is more complicated. That is most clearly seen in the mean velocity maps of  $\text{NH}_3(1,1)$  and (3,3) lines. Most of the emission in the east lobe is blueshifted with respect to the systemic velocity. The northern portion of the east lobe is, however, moving at slower velocities almost the same as the systemic velocity. The kinematics of the west lobe is almost mirror symmetric with respect to the of the east lobe, i.e most of the emission is redshifted with respect to the systemic velocity with the southern portion moving at an average velocity close to the systemic velocity. Most likely the east and west lobes consist of multiple kinematic sub-components with very different spatial kinematics. This point will be discussed further in the next section.

## 4. Discussion

### 4.1. Line ratios

The inversion transitions of NH<sub>3</sub> have been widely used to gauge the physical conditions in different environments, especially in starforming regions. Therefore our observations of multilines in the Egg nebula can be used to infer the physical conditions of the molecular gas through the excitation analysis. More specifically, the gas temperature can be estimated from the line ratios together with some plausible assumptions. We form the line ratio maps (2,2)/(1,1) and (3,3)/(1,1) by convolving the channel maps to the same angular resolution of 4".1 and then producing the integrated intensity maps and then the line ratio maps. The line ratio maps are shown in Figures 8 and 9. Surprisingly, the spatial distribution of the two line ratios is very similar. Although the east and west lobe are stronger in the integrated intensity maps, the line ratios there are generally low, ranging from about 0.3 to 0.9 for both NH<sub>3</sub>(2,2)/(1,1) and NH<sub>3</sub>(3,3)/(1,1). In contrast, the line ratios are generally higher in the polar direction, ranging from 0.8 up to 1.4 for both cases. Because the excitation of higher lying transitions NH<sub>3</sub>(2,2) and (3,3) requires hot and dense gas, high line ratios in the polar direction suggests that the molecular gas in the polar lobes is both hotter and denser in comparison to the molecular gas present in the equatorial plane.

If we assume that the NH<sub>3</sub> inversion lines are optically thin, the opacity ratio for any pair of lines can be calculated as follows (Ho & Townes 1983):

$$\frac{\tau(J', K')}{\tau(J, K)} = \frac{\nu^2(J', K')}{\nu^2(J, K)} \frac{\Delta\nu(J', K')}{\Delta\nu(J, K)} \frac{T_{ex}(J, K)}{T_{ex}(J', K')} \frac{|\mu(J', K')|^2}{|\mu(J, K)|^2} \frac{g(J', K')}{g(J, K)} \times \exp \left\{ \frac{-\Delta E(J', K'; J, K)}{kT_R(J', K'; J, K)} \right\}, \quad (1)$$

where  $T_{ex}(J, K)$  is the excitation temperature of the inversion line,  $|\mu(J, K)|^2 = \mu^2 K^2 / [J(J+1)]$  are the dipole matrix elements,  $g(J, K)$  is the statistical weight,  $g(J, K) = g_{op}(2J+1)$ , with  $g_{op} = 1$  for para-ammonia levels ( $J = 1, 2, 4, 5, 7, 8, \dots$ ) and  $g_{op} = 2$  for ortho-ammonia levels ( $J = 0, 3, 6, \dots$ ).  $\Delta E(J', K'; J, K)/k$  is the energy difference between two states ( $J', K'$ ) and ( $J, K$ ). In the optically thin limit, we can use the line ratio to estimate the rotation temperature  $T_R$  between states ( $J, K$ ) and ( $J', K'$ ), which is a good indicator of the gas temperature  $T_K$ . The rotation temperature can be calculated from the following expression (Menten & Alcolea 1995):

$$T_R(J', K'; J, K) = \left[ \frac{E(J', K') - E(J, K)}{k} \right] \left\{ \ln \left[ \frac{\int T_b(J, K) dv}{\int T_b(J', K') dv} \frac{J(J+1)K'^2(2J+1)g'_{op}}{J'(J'+1)K^2(2J+1)g_{op}} \right] \right\}^{-1} \quad (2)$$

The energy difference between (2,2) and (1,1) states is 41.2 K and that for (3,3) and (1,1) states is 100.3 K, respectively (Menten & Alcolea 1995). From the values of the (2,2)/(1,1) ratio mentioned above we estimate that the rotation temperature  $T_R(2,2;1,1)$  ranges between  $\sim 21$  to 46 K in the east and west lobes. In the polar direction the rotation temperature  $T_R(2,2;1,1)$  can reach as high as 90 K because of the higher line ratio. Similarly, we find that the rotation temperature  $T_R(3,3;1,1)$  is in the range between 32 to 50 K in the east and west lobes and reaches higher value up to 62 K in the polar direction. We note that the high rotation temperatures derived here are broadly consistent with our optically thin assumption for the inversion lines of  $\text{NH}_3$ . As we can see from the channel maps of (1,1), (2,2) and (3,3) lines, the brightness temperature is in the range 1 to 4 K, even though the emitting regions are spatially resolved. Thus the inversion lines are likely optically thin if the excitation temperatures  $T_{\text{ex}}(J,K)$  is comparable to the derived rotation temperatures. We caution, however, that the rotation temperature between ortho-ammonia state (3,3) and the para-ammonia state (1,1) is of limited meaning because of the selection rule that forbids any radiative or collisional transition connecting between the ortho and para states (Ho & Townes 1983).

#### 4.2. Association of $\text{NH}_3$ emission with shocked molecular gas

The complex morphology and spatial kinematics of ammonia emission indicate that ammonia emission does not originate from the unshocked remnant AGB wind. Instead, there are several lines of evidences suggesting that the emission is associated with the shocked molecular gas produced by the interaction between high velocity jets and the slowing expanding shell ejected when the central star was still on the AGB phase.

From high angular resolution observations of CO J=2–1 line, Cox et al. (2000) identify a series of high velocity molecular outflows in the Egg nebula. These outflows are oriented in the polar axis and in the equatorial direction. More interestingly, these outflows can be traced back to a common origin close to the center of the nebula. In Figures 4, 5 and 6 we overlay the location of the molecular outflows identified by Cox et al. (2000) on the integrated intensity maps of  $\text{NH}_3$  emission. These outflows form a cross-like shape, very similar to the morphology of the  $\text{NH}_3$  emission, and spatially coincide with the location of the four lobes traced by the  $\text{NH}_3$  emission. We also find that the  $\text{NH}_3$  emission covers a similar velocity range (between  $-74$  to  $-4 \text{ km s}^{-1}$ ) as the CO J=2–1 line and exhibits similar spatial kinematics. Namely, the CO emission in the polar direction appears blueshifted in the north and redshifted in the south, as expected from the mean velocity maps of  $\text{NH}_3$ . Similarly, The CO J=2–1 emission associated with outflows in the equatorial direction exhibits blueshifted



emission in the east and redshifted in the west, exactly the same trend seen in the intensity weighted mean velocity maps of  $\text{NH}_3$  emission shown in Figures 5, 6 and 7.

The kinematics of strong molecular hydrogen emission at  $2.2 \mu\text{m}$ , which is commonly believed to trace the shocked gas, has been shown by Kastner et al. (2001) to be similar to that seen in CO J=2–1 emission. In addition, in the equatorial direction, the prominent and extended molecular hydrogen emission in the east, which exhibits blueshifted velocities, can be separated into three distinct sub-components with different spatial kinematics. Among the three sub-component E2, E3 and E4 in the terminology of Sahai et al. (1998b), the E4 sub-component located to the north is moving more slowly than other sub-components. Comparison with the mean velocity maps of  $\text{NH}_3$  emission we also see that the northern portion of the east lobe has lower average velocity, almost the same as the systemic velocity. Kastner et al. (2001) propose that the spatial kinematics of the molecular hydrogen emission could result from rotation in the equatorial plane of the Egg nebula. A similar suggestion was made early by Bieging & Nguyen-Q-Rieu (1996) based on their observations of the HCN J=1–0 line. However, our current observations, which have similar spatial and velocity resolution, do not add any new information to either support or disprove the suggestion of rotation in the equatorial plane in the Egg nebula.

The similarity in spatial distribution and kinematics observed in molecular hydrogen emission and  $\text{NH}_3$  inversion transitions strongly suggest that the  $\text{NH}_3$  emission originates from the shocked molecular gas. We note, however, that the molecular hydrogen emission arises from molecular gas at temperature at least as high as 1000 – 2000 K, whereas the  $\text{NH}_3$  emission is coming from much lower temperature gas as suggested by the low rotation temperatures of the inversion lines estimated in the previous section. This would imply a large temperature gradient within the shocked region and the emission lines from either molecular hydrogen or  $\text{NH}_3$  would trace the temperature range most favorable to the their excitation.

### 4.3. Is the abundance of ammonia enhanced in shocks ?

The strong ammonia emission associated with the shocked molecular gas and the lack of emission at the center of the Egg nebula suggest that most of the ammonia did not formed initially in the AGB wind but is produced in the shocked gas. Generally,  $\text{NH}_3$  is not thought to form through gas-phase chemistry in the dusty wind of AGB stars. In chemical models for circumstellar envelopes,  $\text{NH}_3$  is either not considered (Glassgold et al. 1986, Cherchneff et al. 1993) or assumed to formed initially in the stellar atmosphere and injected into the wind (Millar & Herbst 1994). Willacy & Cherchneff (1998) considered the effect of shock

processing on the molecular abundances for the case of the prototypical carbon rich AGB star IRC+10216. However, the number abundance of  $\text{NH}_3$  (relative to  $\text{H}_2$ ) even in that case remains very low, up to only about a few  $10^{-11}$ . Nejad et al. (1990) and Flower et al. (1995) suggest that the  $\text{NH}_3$  molecules might form through surface chemistry on dust grains and remain on the grain surface until the release by the passage of shocks. In their model, a shock velocity in the range 10 to 15  $\text{km s}^{-1}$  would heat up the gas and lead to the release of  $\text{NH}_3$  from the dust grain mantles. The theoretical calculations of Burton et al. (1992) indicate that a minimum shock velocity of about 10  $\text{kms}^{-1}$  is necessary to excite the molecular hydrogen 2.2  $\mu\text{m}$  line. The observations of strong molecular hydrogen 2.2  $\mu\text{m}$  emission in the Egg nebula (Sahai et al. 1998b) suggest that the strength of the shocks in the Egg nebula is comparable or even stronger than needed in the abovementioned chemical models in order to produce the abundance enhancement of  $\text{NH}_3$ . In addition, the relatively high rotation temperatures estimated from the ratio of ammonia inversion lines also favors this scenario in the Egg nebula. We note that similar observations of the enhanced ammonia emission in the bipolar outflows from young stellar objects. For L1155 outflow, Tafalla & Bachiller (1995) found very good spatial coincidence between ammonia emission and the distribution of SiO J=2–1 line, which is considered as a good tracer of the shocked gas. Follow up observations by Umemoto et al. (1999) revealed the emission from highly excited (5,5) and (6,6) inversion lines. The high rotational temperature of ammonia molecules as well as the significant departure of the ortho–para ratio from the statistical equilibrium value point to the evaporation of  $\text{NH}_3$  from the surface of dust grains following the passage of shocks.

Given the relatively well constrained geometry and physical conditions inside the Egg nebula, more elaborate models should be attempted to explore further the formation and excitation of ammonia in the shock regions.

## 5. Conclusion

In this paper we have imaged at high angular resolution the emission of  $\text{NH}_3(1,1)$ , (2,2) and (3,3) inversion lines from the Egg Nebula. We find that the spatial distribution and kinematics of the emission in all three lines show four distinct components or lobes that are aligned with the polar and equatorial directions. The kinematics of the  $\text{NH}_3$  emission is also found to follow a clear pattern: redshifted emission in the South and West and blueshifted emission in the North and East. The morphology and spatial kinematics of  $\text{NH}_3$  emission are shown to have strong similarity to that observed previously in molecular hydrogen emission and CO emission which arise from the shocked molecular gas. We also find that the higher lying inversion transition  $\text{NH}_3$  (2,2) and (3,3) are stronger in the polar

direction in comparison to the lower transition  $\text{NH}_3$  (1,1). We conclude that the  $\text{NH}_3$  emission traces the warm molecular gas, which is shocked and heated by the interaction between the high velocity outflows and the surrounding envelope. From the association of  $\text{NH}_3$  emission with the shocked molecular gas and the lack of the emission at the center of the nebula we conclude that the abundance of ammonia is significantly enhanced by shocks, a situation very similar to that found in outflows from protostars.

We thank an anonymous referee for insightful and constructive comments that help to improve the presentation of our paper. We also thank the VLA staff for their help with the observations. This research has made use of NASA's Astrophysics Data System Bibliographic Services and the SIMBAD database, operated at CDS, Strasbourg, France.

## REFERENCES

- Bieging, J.H., Nguyen-Q-Rieu, 1996, *AJ* 112, 706
- Burton, M.G., Hollenbach, D.J., Tielens, A.G.G.M., 1992, *ApJ* 399, 563
- Cherchneff, I., Glassgold, A.E., Mamon, G.A., 1993, *ApJ* 410, 188
- Cox, P., Lucas, R., Huggins, P.J., Forveille, T., Bachiller, R., Guilloteau, S., Maillard, J.P., Omont, A., 2000, *A&A* 353, L25
- Flower, D.R., Pineau des Forêts, G., Walmsley, C.M., 1995, *A&A* 294, 815
- Glassgold, A.E., Lucas, R., Omont, A., 1986, *A&A* 157, 35
- Hasegawa, T.I., Kwok, S., Koning, N., et al., 2006, *ApJ* 637, 791
- Ho, P.T.P., Townes, C.H., 1983, *ARAA* 21, 239
- Jura, M., Kroto, H., 1990, *ApJ* 351, 222
- Jura, M., Turner, J.L., van Dyk, S., Knapp, G.R., 2001, *ApJ* 528, L105
- Kastner, J.H., Weintraub, D.A., Gatley, I., Henn, L.A., 2001, *ApJ* 546, 279
- Klochkova, V.G., Szczerba, R., Panchuck, V.E., 2000, *Astr. Lett.*, 26, 439
- Kukolich, S., 1967, *Phys. Rev.* 156, 83
- Menten, K., Alcolea, J., 1995, *ApJ* 448, 416

- Millar, T.J., Herbst, E., 1994, A&A 288, 561
- Nejad, L.A.M., Williams, D.A., Charnley, S.B., 1990, MNRAS 246, 183
- Nguyen-Q-Rieu, Graham, D., Bujarrabal, V., 1984, A&A 138, L5
- Nguyen-Q-Rieu, Winnberg, A., Bujarrabal, V., 1986, A&A 165, 204
- Rydbeck, O.E.H., et al., 1977, ApJ 215, L35
- Sahai, R., Trauger, J.T., Watson, A.M., et al. 1998, ApJ 493, 301
- Sahai, R., Hines, D., Kastner, J.H., et al., 1998, ApJ 492, L163
- Tafalla, M., Bachiller, R., 1995, ApJ 443, L37
- Truong-Bach, Graham, D., Nguyen-Q-Rieu, 1988, A&A 199, 291
- Ueta, T., Murakawa, K., Meixner, M., 2006, ApJ 641, 1113
- Umemoto, T., Mikami, H., Yamamoto, S., Hirano, N., 1999, ApJ 525, L105
- Walmsley, C.M., Ungerechts, H., 1983, A&A 122, 164
- Willacy, K., Cherchneff, I., 1998, A&A 330, 676
- Young, K., Serabyn, G., Phillips, T.G., Knapp, G.R., Guesten, R., Schulz, A., 1992, ApJ 385, 265

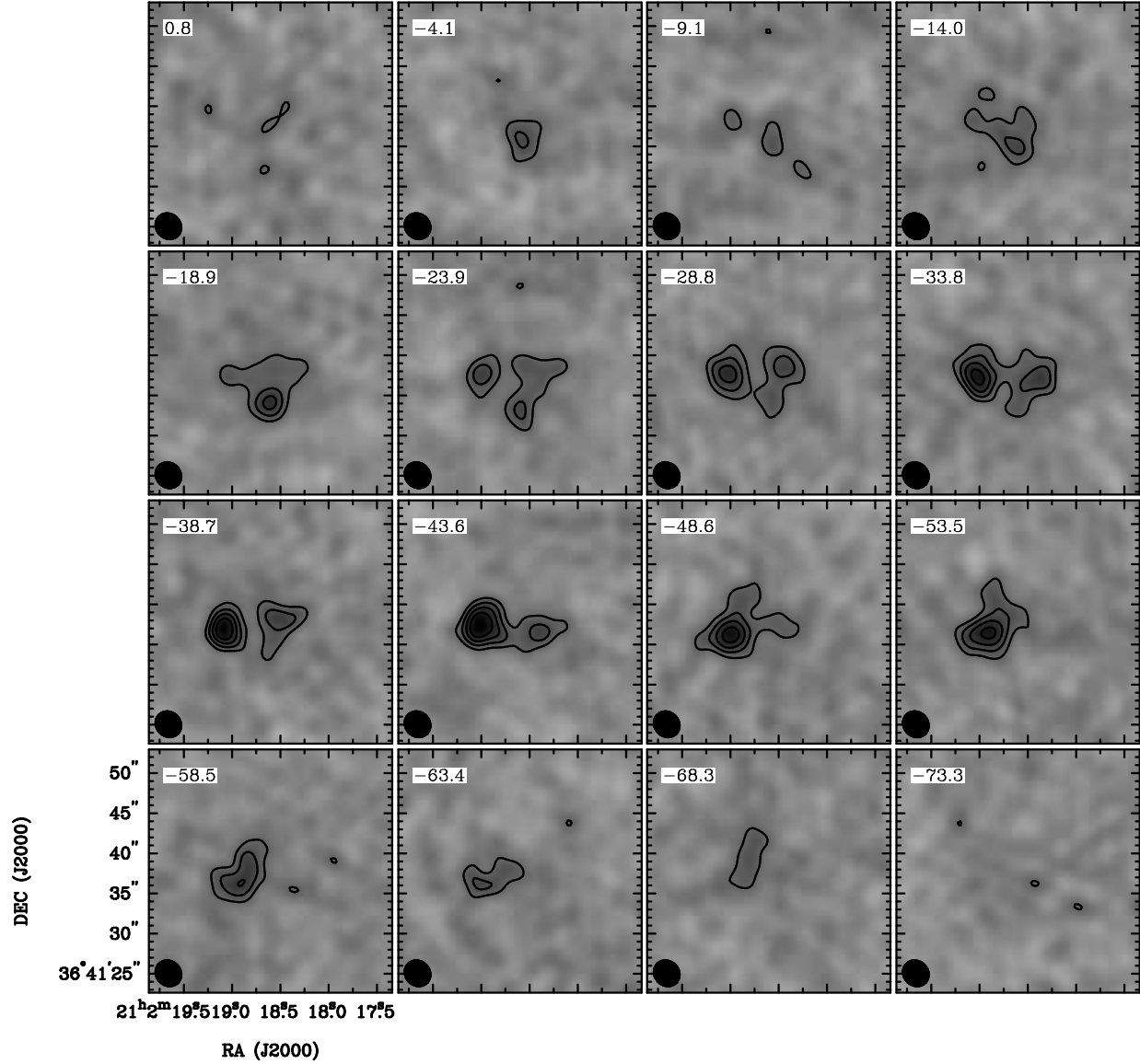


Fig. 1.— Channel maps of the  $\text{NH}_3(1,1)$  emission from the Egg nebula in contour and grayscale. The contour levels are (3, 5, 7, 9, 12) $\sigma$  where the rms noise level  $\sigma = 2.0$  mJy beam $^{-1}$ . The synthesise beam of  $3''.5 \times 3''.1$  is shown in the lower left of the upper left frame. The conversion factor between the brightness temperature and the flux of the  $\text{NH}_3(1,1)$  emission is 5 mJy K $^{-1}$ .

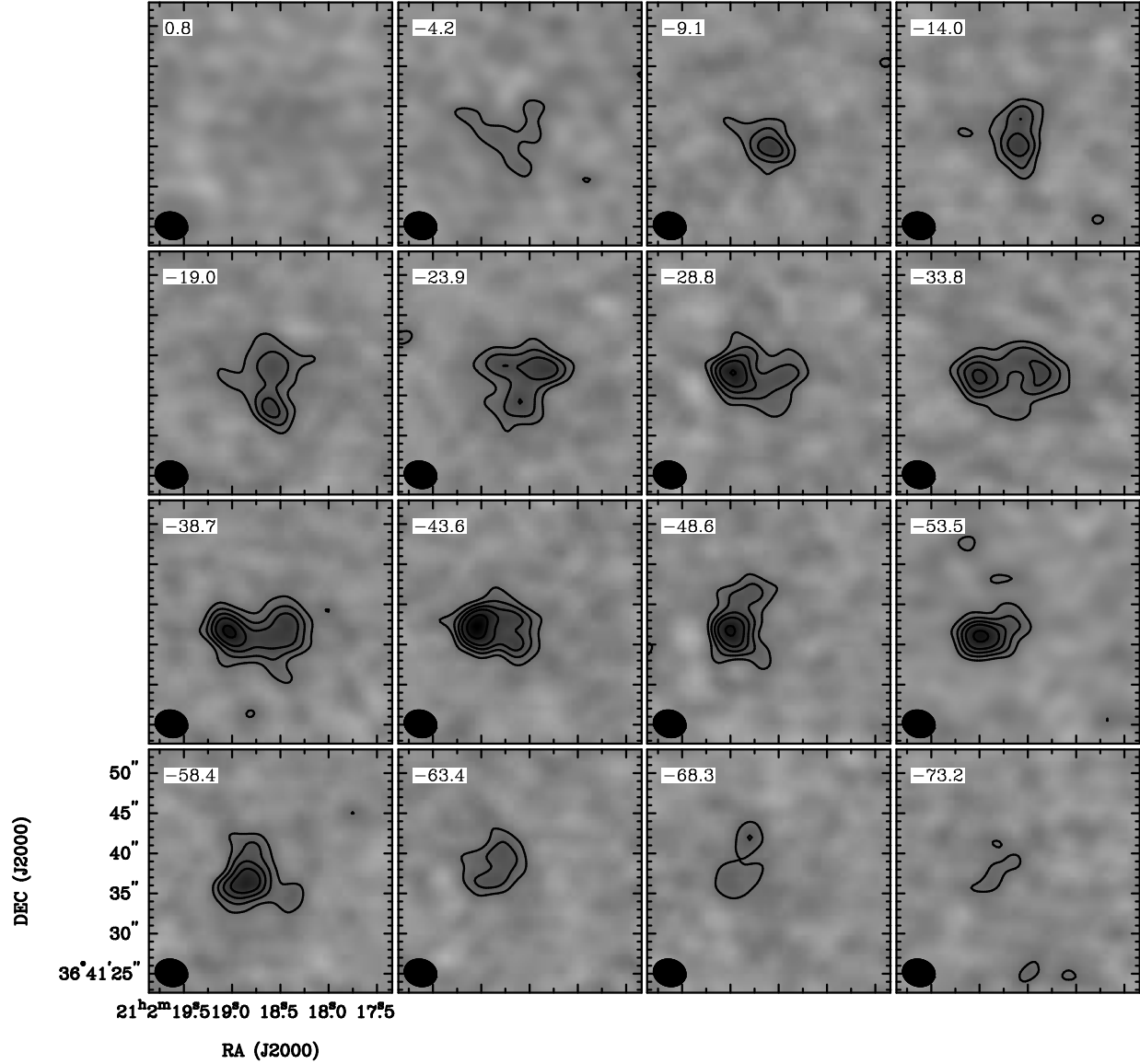


Fig. 2.— Channel maps of the  $\text{NH}_3(2,2)$  emission from the Egg nebula in contour and grayscale. The contour levels are (3, 5, 7, 9, 12) $\sigma$  where the rms noise level  $\sigma = 1.5$  mJy beam $^{-1}$ . The synthesise beam of  $4''.1 \times 3''.4$  is shown in the lower left of the upper left frame. The conversion factor between the brightness temperature and the flux of the  $\text{NH}_3(2,2)$  emission is  $6.4$  mJy  $\text{K}^{-1}$ .

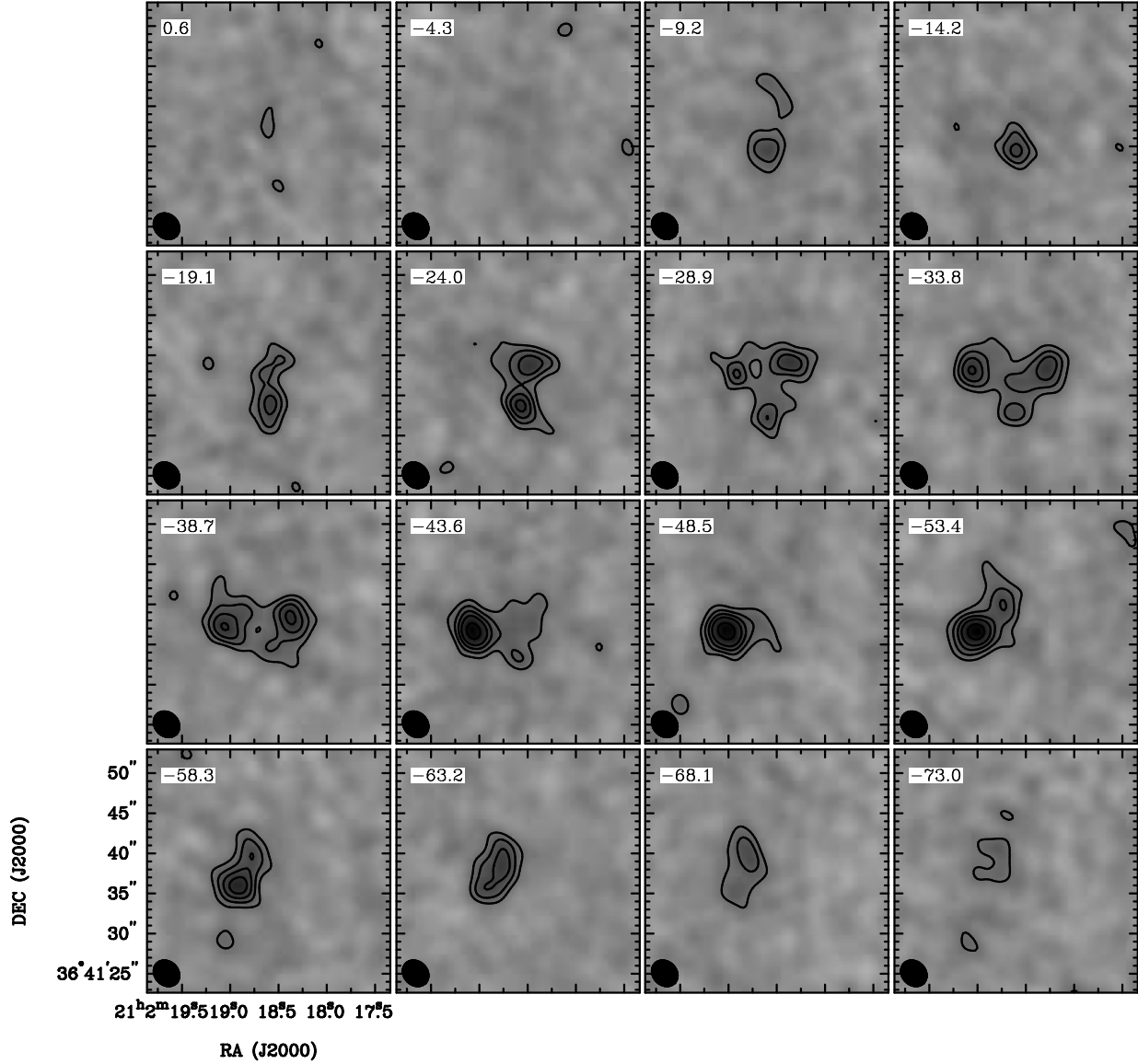


Fig. 3.— Channel maps of the  $\text{NH}_3(3,3)$  emission from the Egg nebula in contour and grayscale. The contour levels are (3, 5, 7, 9, 12) $\sigma$  where the rms noise level  $\sigma = 1.5 \text{ mJy beam}^{-1}$ . The synthesizer beam of  $3''.6 \times 3''$  is shown in the lower left of the upper left frame. The conversion factor between the brightness temperature and the flux of the  $\text{NH}_3(3,3)$  emission is  $5 \text{ mJy K}^{-1}$ .

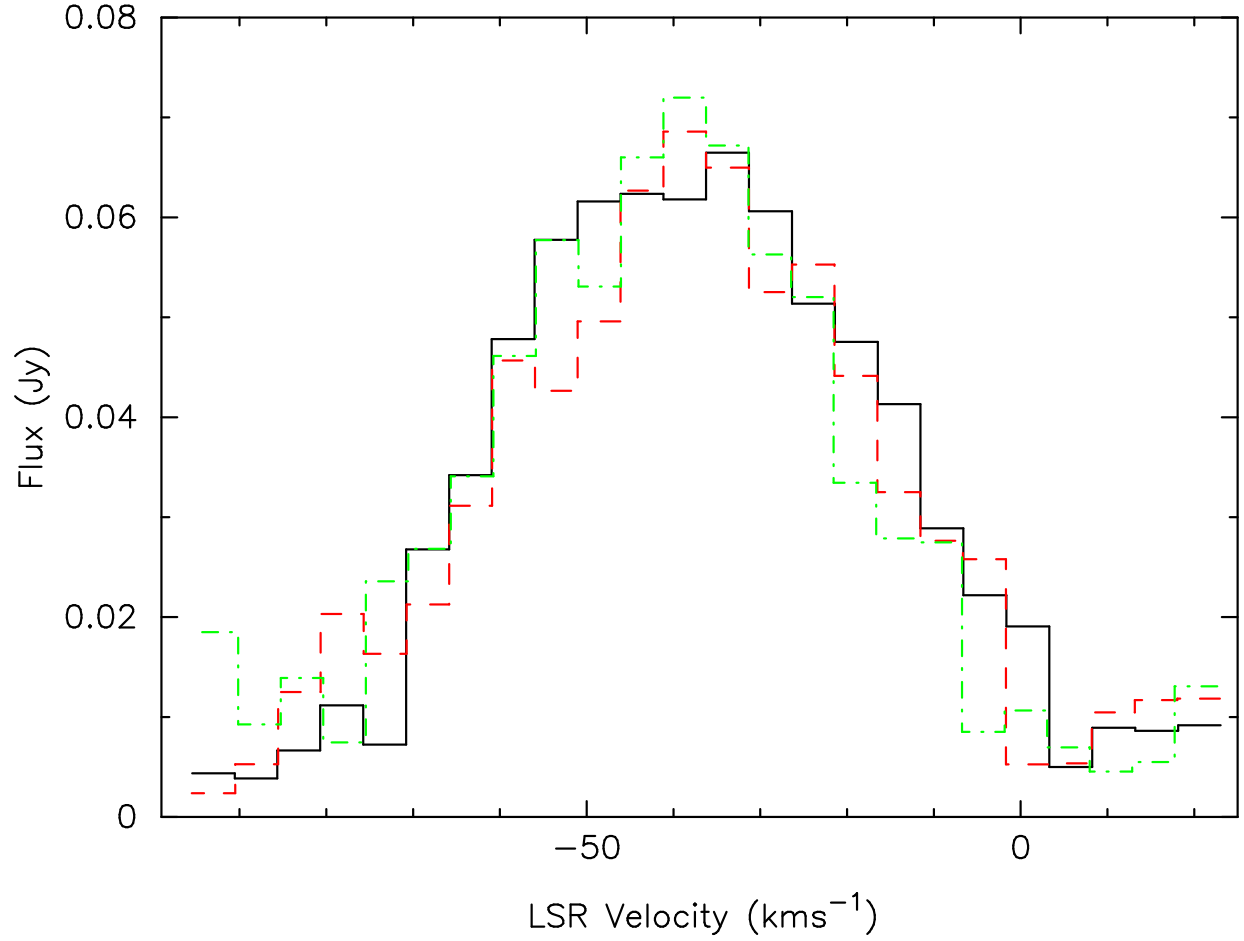


Fig. 4.— Total intensity profiles of the  $\text{NH}_3$  (1,1) transition, shown in black solid line, (2,2) transition, shown in dashed line, and (3,3) transition, shown in dashed-dotted line, from the Egg nebula.



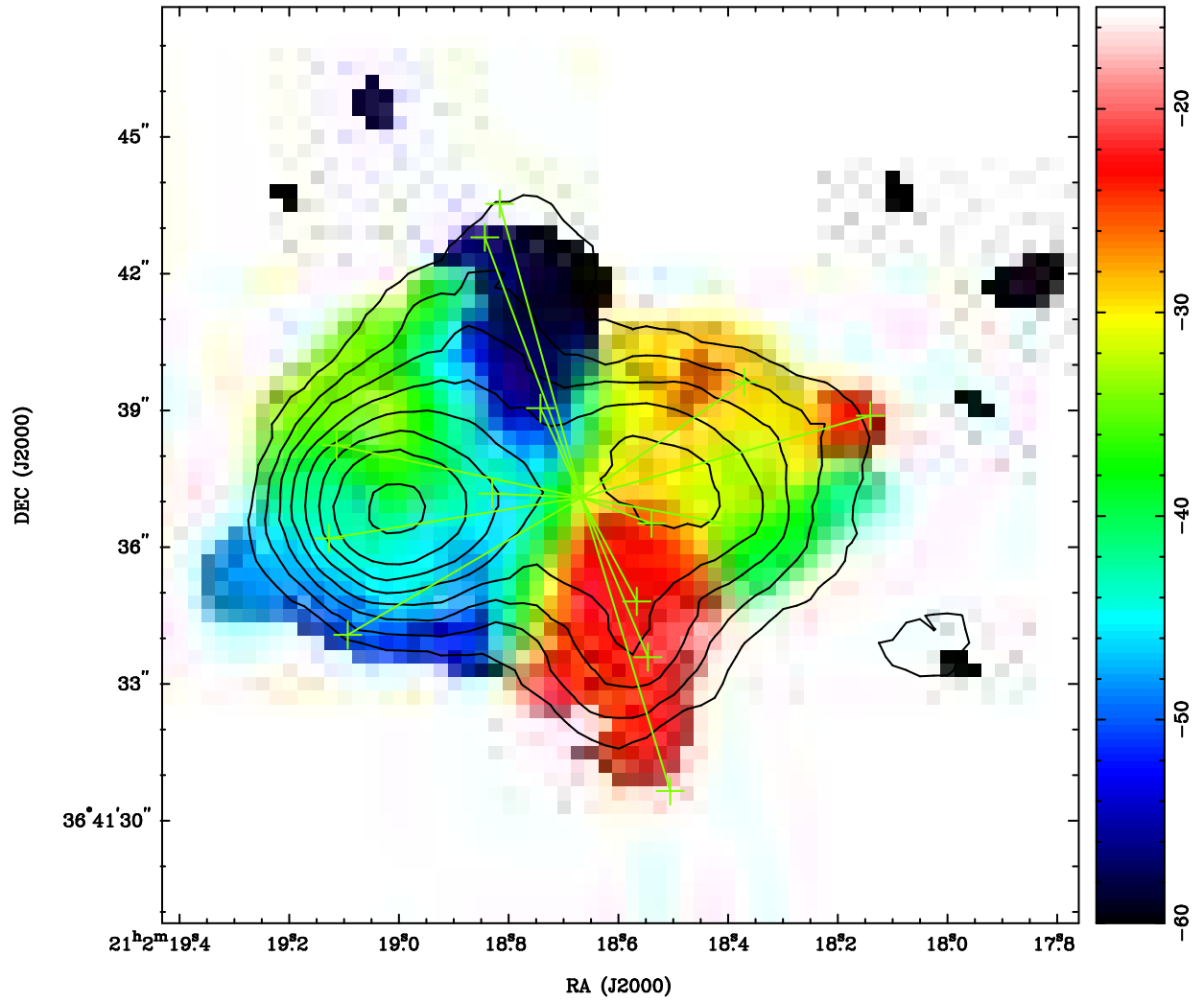


Fig. 5.— The integrated intensity map of the  $\text{NH}_3(1,1)$  line from the Egg nebula. The contour levels start from  $(0.2 \text{ to } 0.8 \text{ in step of } 0.2 \text{ and } 0.95) \times 0.9 \text{ Jy km s}^{-1}$ . The high velocity jets identified by Cox et al. (2000) are marked with solid lines.

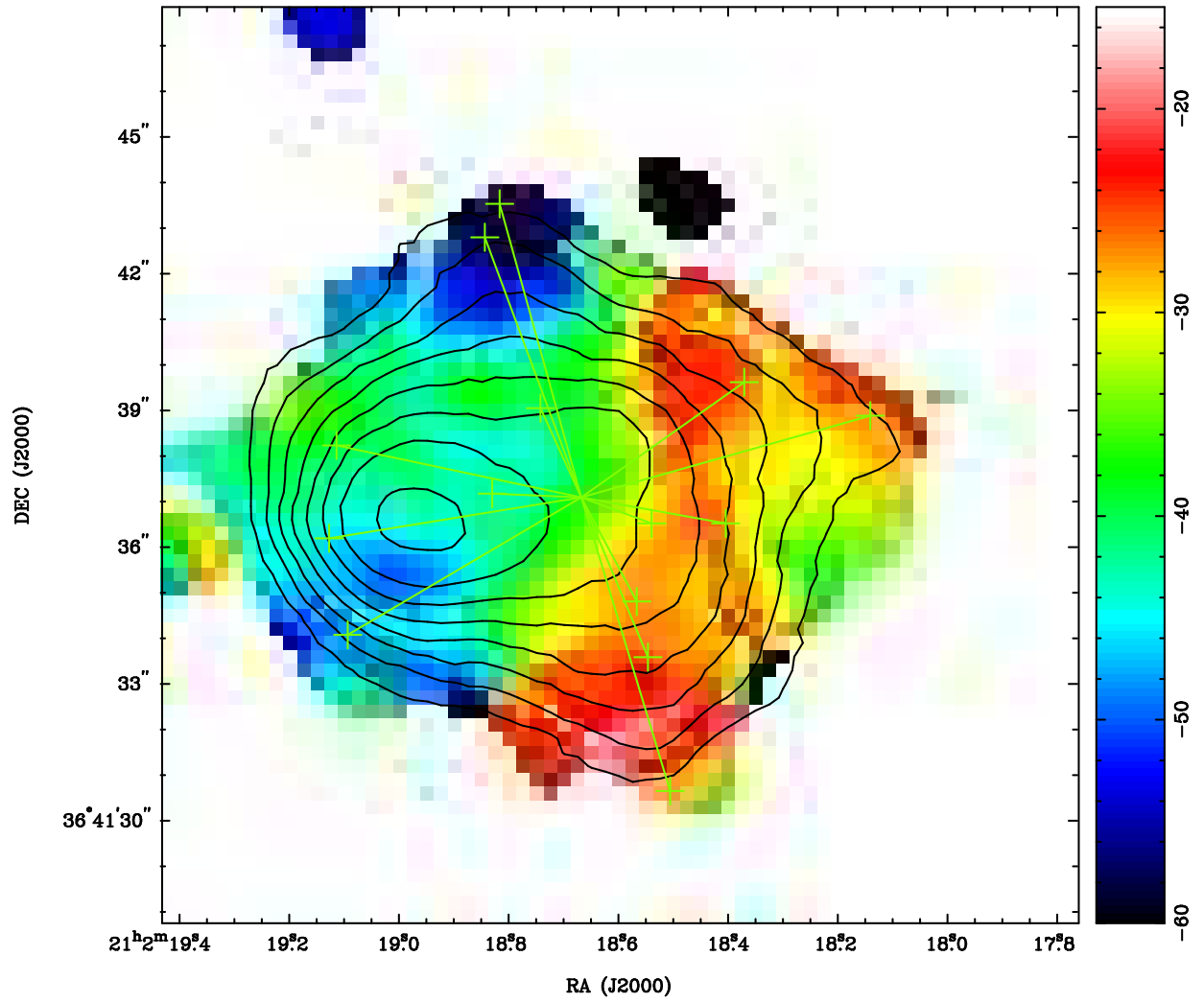


Fig. 6.— The integrated intensity map of the  $\text{NH}_3(2,2)$  line from the Egg nebula. The contour levels start from  $(0.1 \text{ to } 0.8 \text{ in step of } 0.2 \text{ and } 0.95) \times 0.83 \text{ Jy km s}^{-1}$ . The high velocity jets identified by Cox et al. (2000) are marked with solid lines.

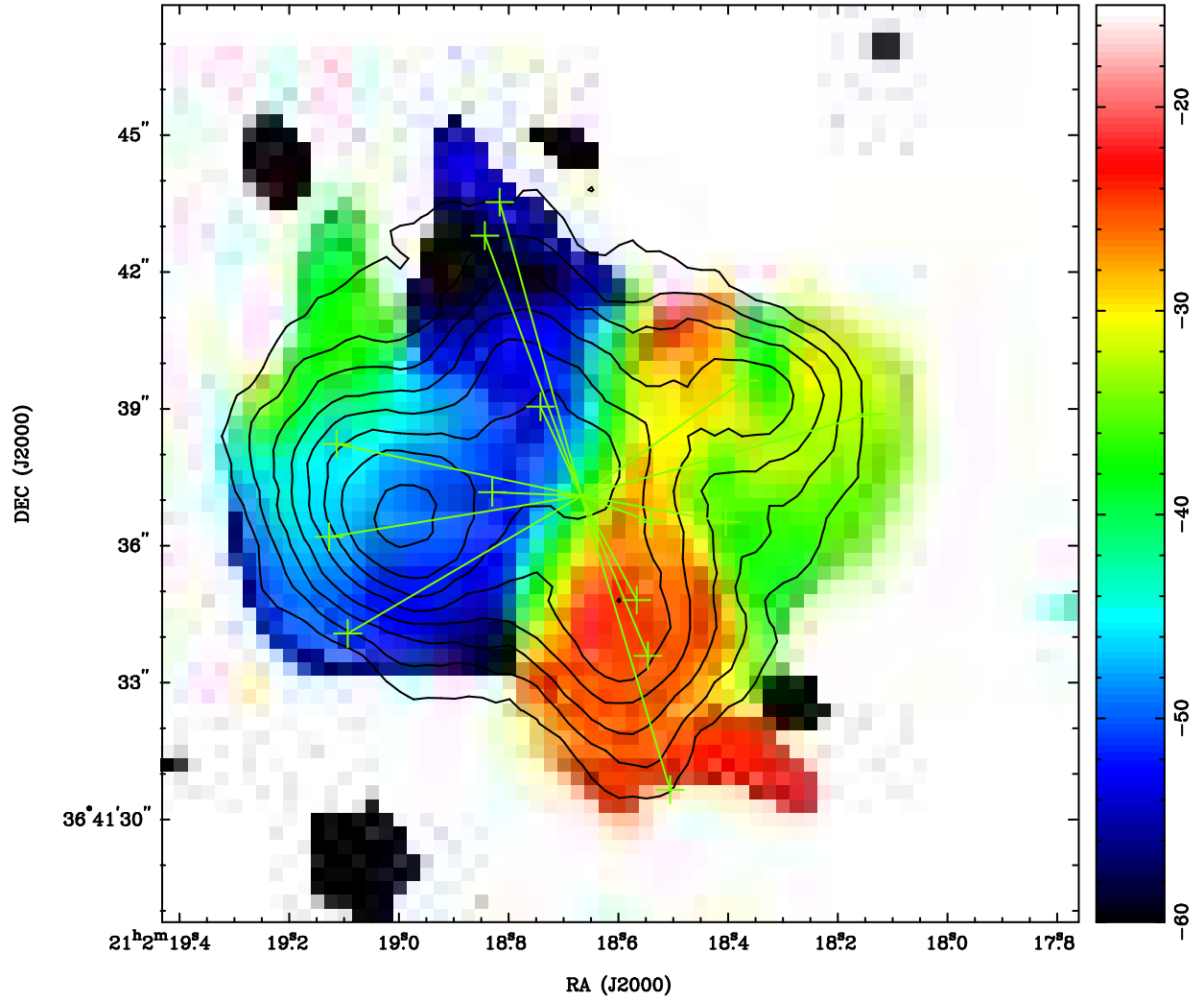


Fig. 7.— The integrated intensity map of the  $\text{NH}_3(3,3)$  line from the Egg nebula. The contour levels start from  $(0.2 \text{ to } 0.8 \text{ by step of } 0.2 \text{ and } 0.95) \times 0.67 \text{ Jy km s}^{-1}$ . The high velocity jets identified by Cox et al. (2000) are marked with solid lines.

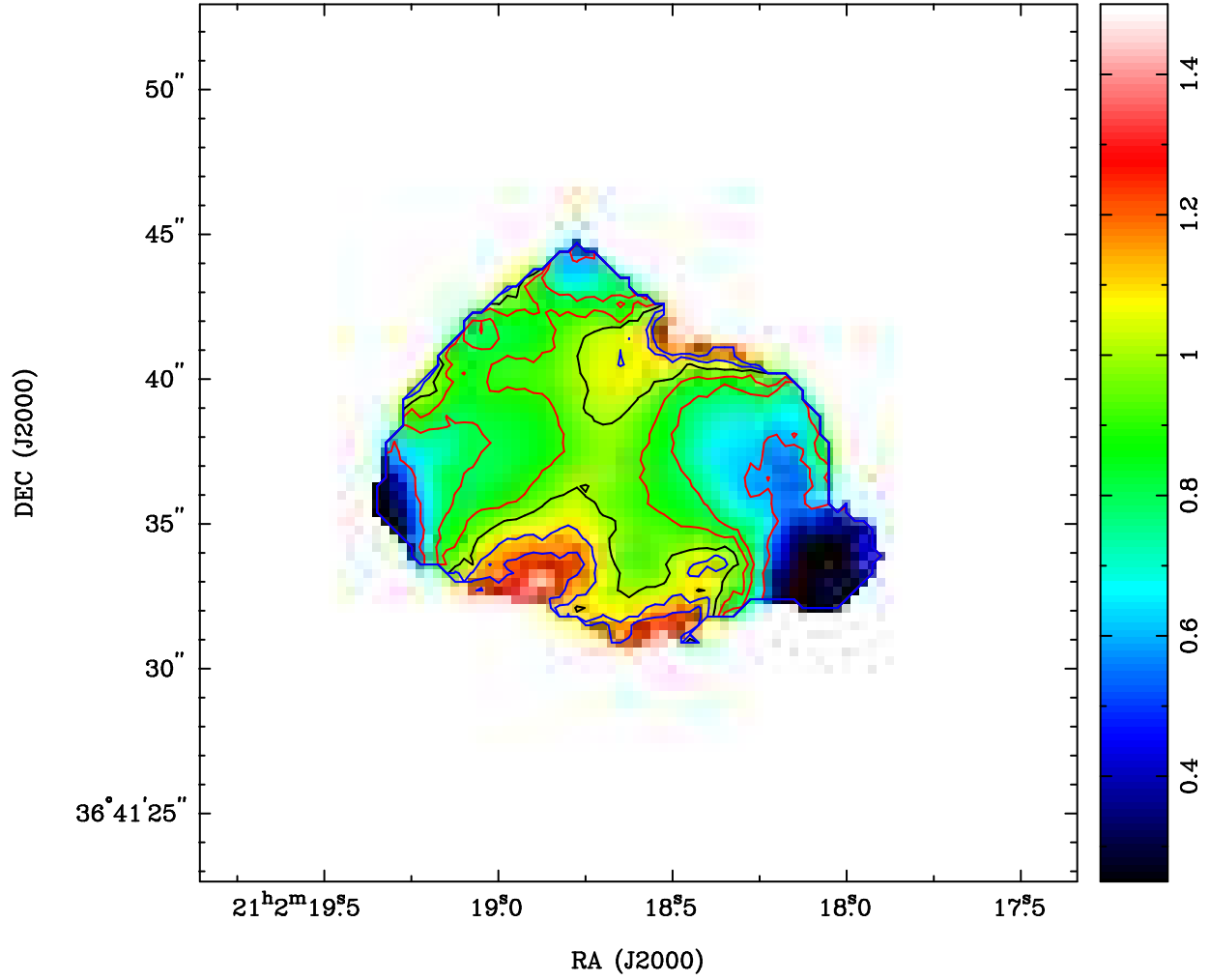


Fig. 8.— The intensity ratio map of the  $\text{NH}_3(2,2)/(1,1)$  line from the Egg nebula. The contour levels are 0.6, 0.8, 0.9, 1, 1.1 and 1.2. The map has an angular resolution of  $4''.1$ .

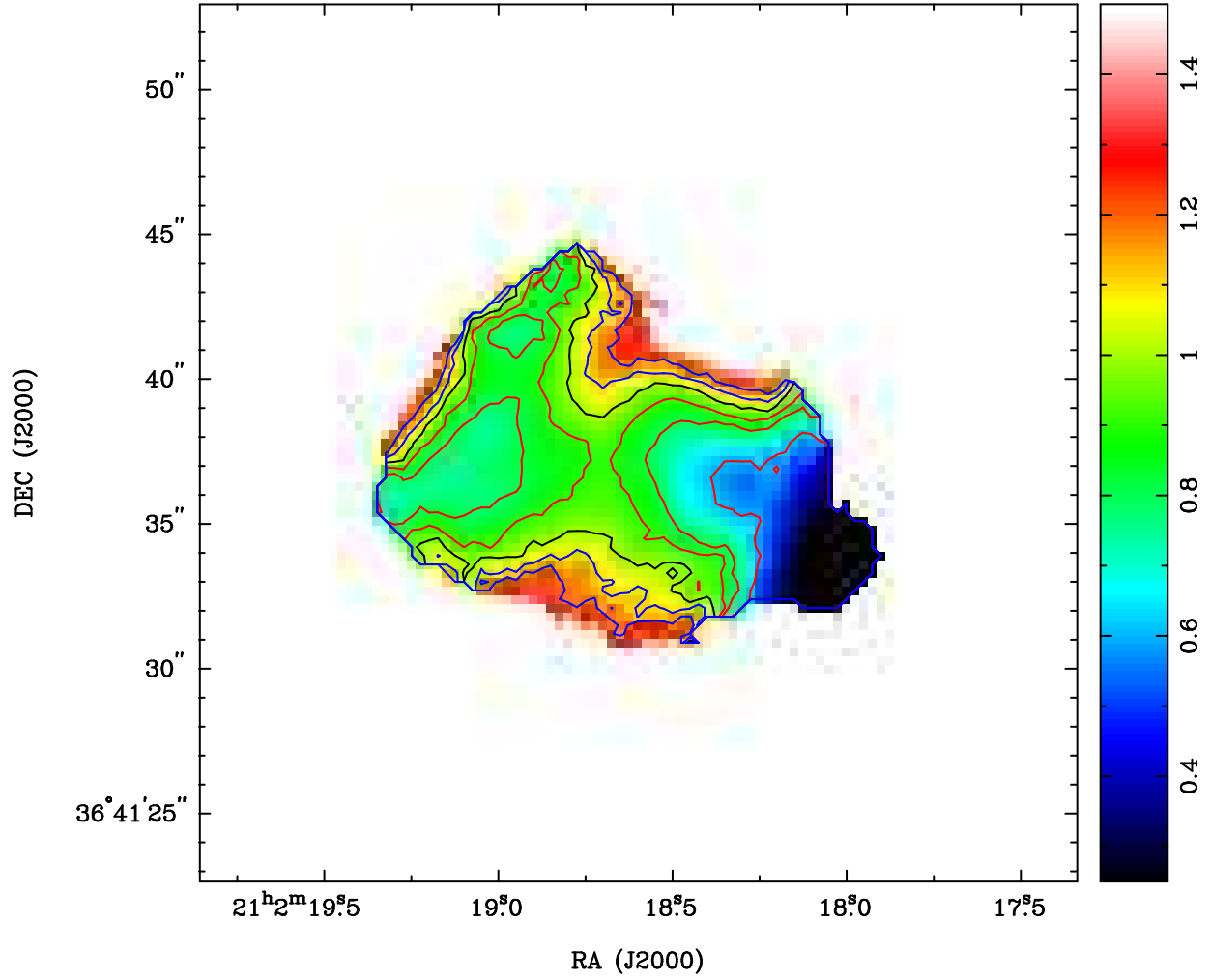


Fig. 9.— The intensity ratio map of the  $\text{NH}_3(3,3)/(1,1)$  line from the Egg nebula. The contour levels are 0.6, 0.8, 0.9, 1, 1.1 and 1.2. The map has an angular resolution of  $4''.1$ .